Bioluminescence Intensity Modeling and Sampling Strategy Optimization*

I. SHULMAN,[+] D. J. MCGILLICUDDY JR.,[#] M. A. MOLINE,[@] S. H. D. HADDOCK,[&] J. C. KINDLE,[+] D. NECHAEV,[**] AND M. W. PHELPS[++]

[+]*Naval Research Laboratory, Stennis Space Center, Mississippi*
[#]*Woods Hole Oceanographic Institution, Woods Hole, Massachusetts*
[@]*California Polytechnic State University, San Luis Obispo, California*
[&]*Monterey Bay Aquarium Research Institute, Moss Landing, California*
[**]*University of Southern Mississippi, Stennis Space Center, Mississippi*
[++]*Jacobs Sverdrup Advanced Systems Group, Stennis Space Center, Mississippi*

(Manuscript received 2 June 2004, in final form 14 December 2004)

ABSTRACT

The focus of this paper is on the development of methodology for short-term (1–3 days) oceanic bioluminescence (BL) predictions and the optimization of spatial and temporal bioluminescence sampling strategies. The approach is based on predictions of bioluminescence with an advection–diffusion–reaction (tracer) model with velocities and diffusivities from a circulation model. In previous research, it was shown that short-term changes in some of the salient features in coastal bioluminescence can be explained and predicted by using this approach. At the same time, it was demonstrated that optimization of bioluminescence sampling prior to the forecast is critical for successful short-term BL predictions with the tracer model. In the present paper, the adjoint to the tracer model is used to study the sensitivity of the modeled bioluminescence distributions to the sampling strategies for BL. The locations and times of bioluminescence sampling prior to the forecast are determined by using the adjoint-based sensitivity maps. The approach is tested with bioluminescence observations collected during August 2000 and 2003 in the Monterey Bay, California, area. During August 2000, BL surveys were collected during a strong wind relaxation event, while in August 2003, BL surveys were conducted during an extended (longer than a week) upwelling-favorable event. The numerical bioluminescence predictability experiments demonstrated a close agreement between observed and model-predicted short-term spatial and temporal changes of the coastal bioluminescence.

1. Introduction

In previous research (Shulman et al. 2003), it was demonstrated that some of the salient short-term changes in bioluminescence (BL) intensity can be explained by hydrodynamic transport processes. Bioluminescence short-term predictability experiments were conducted by assimilating BL observations into an advection–diffusion–reaction (tracer) model with velocities and diffusivities from a circulation model.

The methodology was tested with BL observations acquired during the August 2000 experiment conducted jointly by the Autonomous Ocean Sampling Network (AOSN I), Monterey Bay Aquarium Research Institute (MBARI) Upper-Water-Column Science Experiment (MUSE), and National Oceanic Partnership Program (NOPP) Innovative Coastal-Ocean Observing Network (ICON) projects. The results of numerical experiments designed to estimate the limits of bioluminescence predictions by the tracer model demonstrated the strong utility of the proposed methodology in prediction and interpretation of observed short-term changes (1–3

*Naval Research Laboratory Contribution Number JA/7330-04-10, AOSN Contribution Number 2005.101, and Woods Hole Oceanographic Institution Contribution Number 11253.

Corresponding author address: Igor Shulman, Naval Research Laboratory, Code 7331, Bldg. 1009, Stennis Space Center, MS 39529-5004.
E-mail: igor.shulman@nrlssc.navy.mil

days) in bioluminescence intensity (Shulman et al. 2003).

At the same time, results show that optimization of locations and times of BL observations prior to the forecast are critical for successful short-term BL predictions. It was demonstrated that during a strong wind relaxation event in Monterey Bay, California, the assimilation of only one section of observed BL inside the bay gave a good reconstruction of the location and the maximum of BL observed (not assimilated) outside of the bay. Also, it was shown that sampling of BL outside the bay would provide little information for short-term BL predictability inside the bay. For short-term BL predictability, the sampling of BL intensity should be done in particularly flow-dependent, "sensitive" regions.

Here, short-term BL forecast sensitivities to the circulation patterns, as well as to BL intensity (1–3 days prior to the forecast) are presented. Sensitivity studies were conducted by using the adjoint to the advection–diffusion reaction model. Sensitivity maps illustrate specific areas where initial conditions are most influential on the forecast and where sampling for BL intensity is critical. Bioluminescence sensitivity maps are presented for two extensive BL surveys during the AOSN I (August 2000) and AOSN II (August 2003) experiments. Sensitivity studies were conducted for two major circulation regimes in Monterey Bay—upwelling (August 2003) and relaxation (August 2000). Analysis of the sensitivity maps for August 2000 demonstrated good agreement with BL predictability results presented in Shulman et al. (2003). New BL predictability experiments were conducted utilizing sensitivity maps for the August 2003 experiment.

The paper has the following structure. In section 2, circulation models of the Monterey Bay area are briefly presented. Section 3 describes the observed BL data used in this study. Section 4 discusses the estimation of sensitivity maps with the adjoint and the optimization of BL sampling with sensitivity maps. Bioluminescence predictability experiments during the upwelling event of 2003 are presented in section 5, with conclusions and future plans in section 6.

2. Circulation models

Two circulation models of Monterey Bay are used in this study (Fig. 1). The ICON model has an orthogonal, curvilinear grid with horizontal resolution ranging from 1 to 4 km. The model has 30 vertical sigma levels (Shulman et al. 2002). At the smaller scale, a fine-resolution submodel (frsICON) has been set up within the ICON model domain (Fig. 1). The grid of frsICON has a variable resolution in the horizontal, with a finer resolution (500–600 m) around the upwelling front in the northern part of Monterey Bay telescoping to a coarser resolution (1.5 km) in the outer portion of the domain (Shulman et al. 2003). The ICON and frsICON models are based on the three-dimensional, sigma-coordinate version of the Blumberg and Mellor (1987) hydrodynamic model.

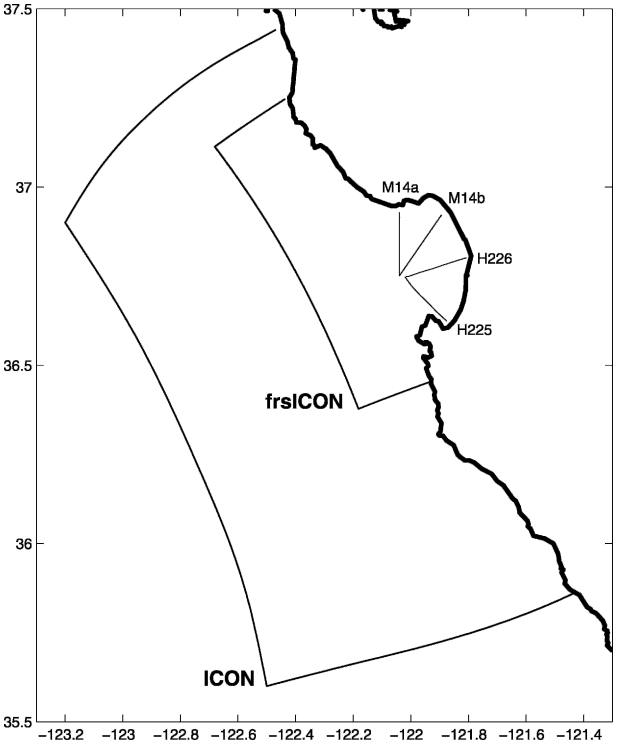

FIG. 1. The ICON and frsICON model domains with the locations of cross sections of bioluminescence observations.

One of the objectives of the numerical simulations during August 2000 was the modeling of the BL intensity. The question of whether short-term changes in some features of BL variability can be explained by hydrodynamic transport processes was investigated. For this reason, the focus of numerical simulations was on accurate model predictions in the upper 100 m of the water column (especially predictions of velocity fields). To achieve this objective, the following important observations and forcings were utilized during the August 2000 and August 2003 simulations:

(a) Models were forced with high-resolution (9 km

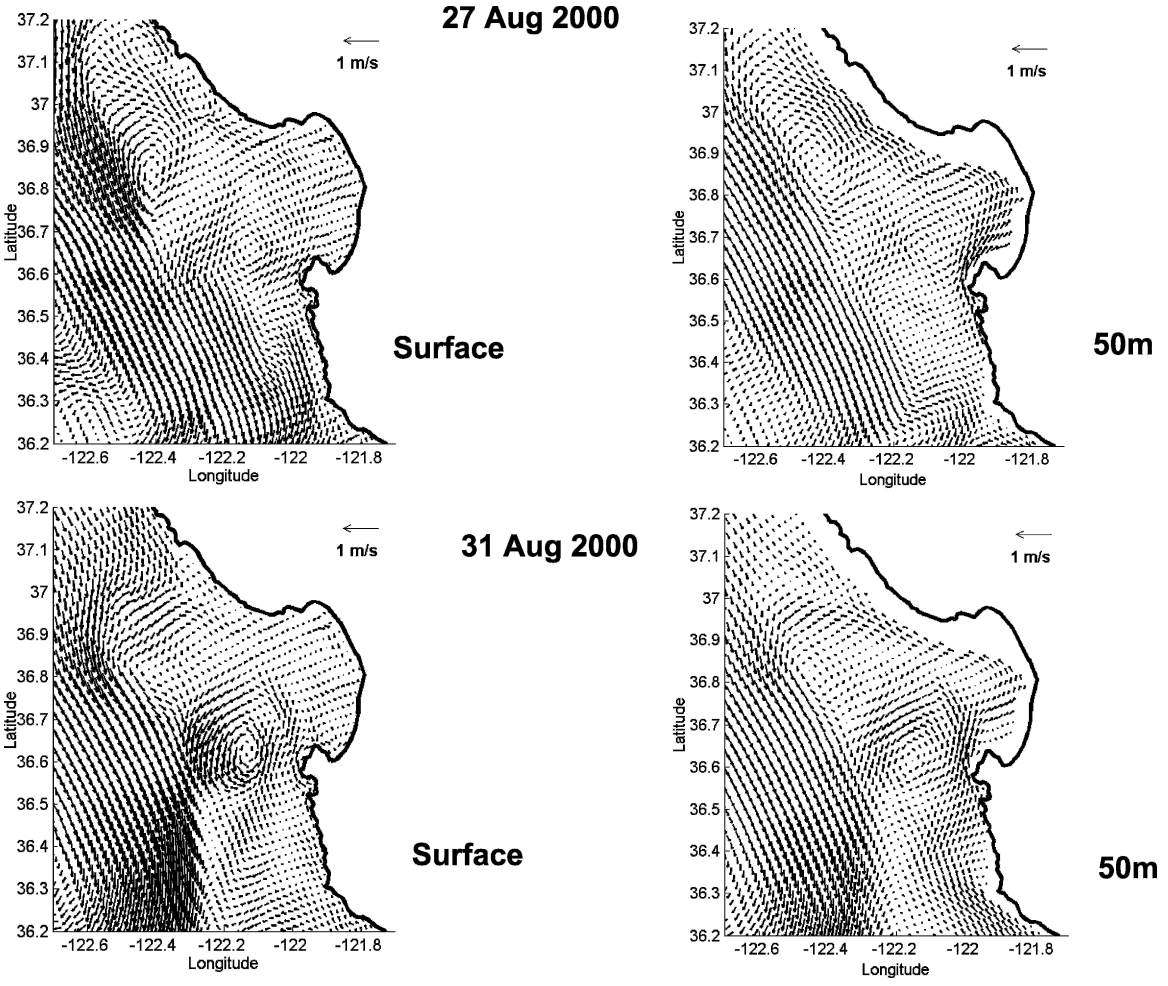

FIG. 2. ICON model surface and 50-m-depth currents during the wind relaxation event of 27–31 Aug 2000.

in August 2000 and 3 km in August 2003) wind stresses and heat fluxes from the Navy Coupled Ocean and Atmospheric Mesoscale Prediction System (COAMPS) (Hodur 1997; Kindle et al. 2002).

(b) High-frequency coastal radar (CODAR) surface currents were assimilated into hydrodynamic models based on the scheme described in Paduan and Shulman (2004).

(c) Open boundary conditions for the ICON model were derived from the larger-scale Pacific West Coast (PWC) model predictions. The PWC model domain extends seaward to 135°W, and from 30° to 49°N. The PWC model was forced with 27-km COAMPS wind forcing, and the multichannel sea surface temperature (MCSST) was assimilated into the PWC model.

During northwesterly, upwelling favorable winds, the hydrographic conditions in and around Monterey Bay are mostly determined by the interaction between upwelling filaments formed at headlands to the north and south of the bay and anticyclonic California Current meander offshore of the bay [see Rosenfeld et al. (1994) for more details]. When upwelling-favorable winds weaken (wind relaxation), and sometimes become poleward, the anticyclonic California Current meander moves onshore and then quickly retreats back offshore when the winds reintensify.

During the relaxation event of August 2000 (Fig. 2), analysis of the ICON model current structure at various depths indicates the development of the nearshore northward flow extending to a depth of 50 m. This northward flow is connected with the northward flow originating at the southern open boundary of the ICON domain (a larger-scale phenomenon generated by the coupling to the PWC model). In

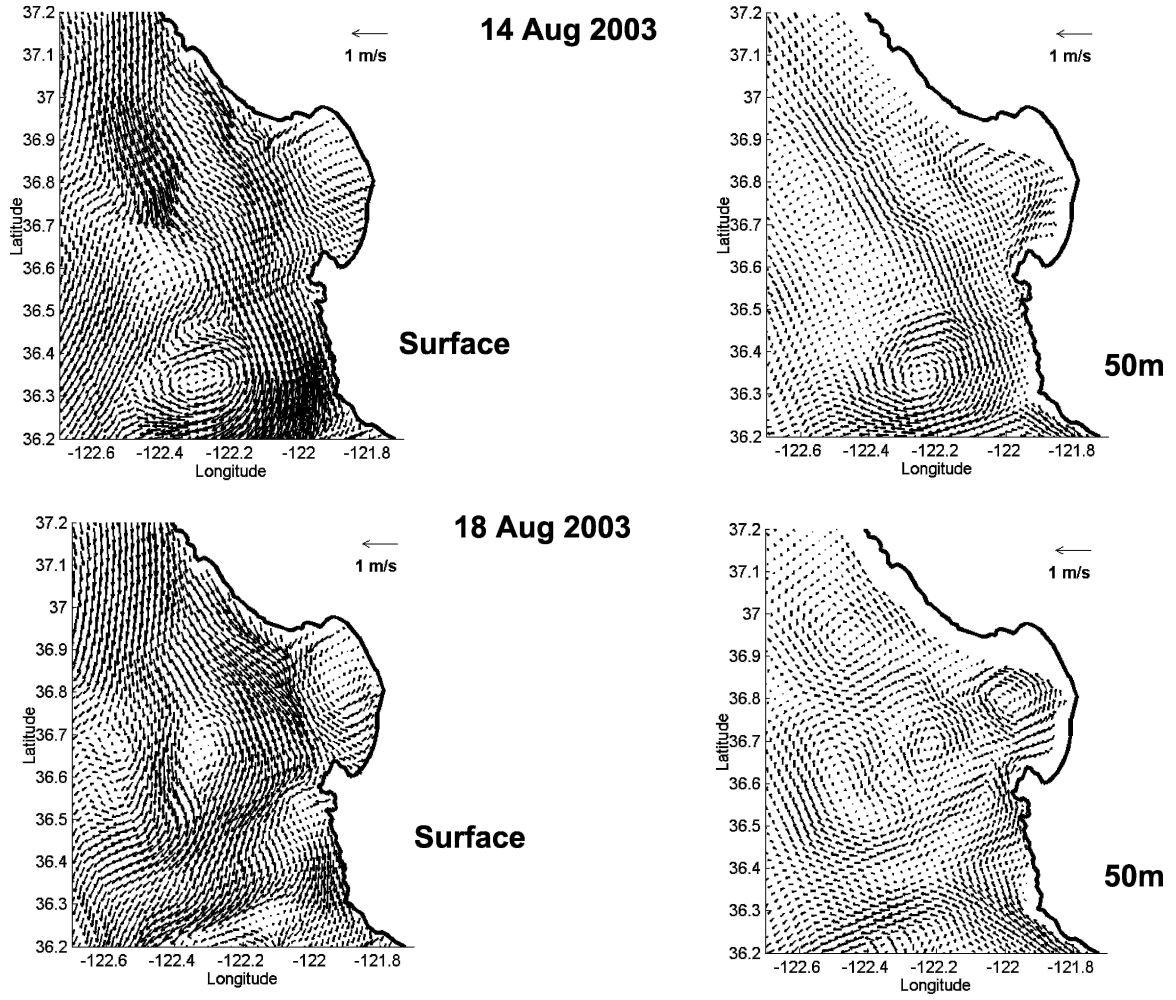

FIG. 3. ICON model surface and 50-m-depth currents during the upwelling event of 14–18 Aug 2003.

the bay, this northward flow develops a cyclonic circulation that is confined between this nearshore northward flow and the southward flow offshore.

Analysis of the ICON model current structure during the upwelling event of August 2003 (Fig. 3) indicates a strong southward-flowing offshore jet. This southward jet intensifies and flows along the entrance to the bay. At the same time, a strong cyclonic eddy is present inside the bay.

3. Bioluminescence observations

Bioluminescence data in Monterey Bay was collected at night during August 2003. The BL was measured using two custom-built bathyphotometers, each mounted on a two autonomous underwater vehicles (AUVs). Both AUVs [a Remote Environmental Measuring Units (REMUS) (Moline et al. 2005) and a Dorado (Wilcox et al. 2001)] proceeded through the water along a preprogrammed path, undulating between shallow (2 m) and deep depth boundaries (40 m). Within each vehicle, in addition to the core instrument packages, a bioluminescence bathyphotometer (Herren et al. 2004) pumps water into a 0.5-L sample chamber at a rate of 0.5 L s^{-1}. Flow rate, temperature, and light levels (photon flux, assuming isotropic emission) are measured in the sample chamber. The instrument is calibrated both radiometrically by a known light source and biologically by insertion of a known concentration of dinoflagellates. As with all bathyphotometers, only a fraction of the total luminescence is stimulated or sampled, but because organisms emit most of their light in the first part of their first flash, we capture a repeatable and representative fraction of the bioluminescence

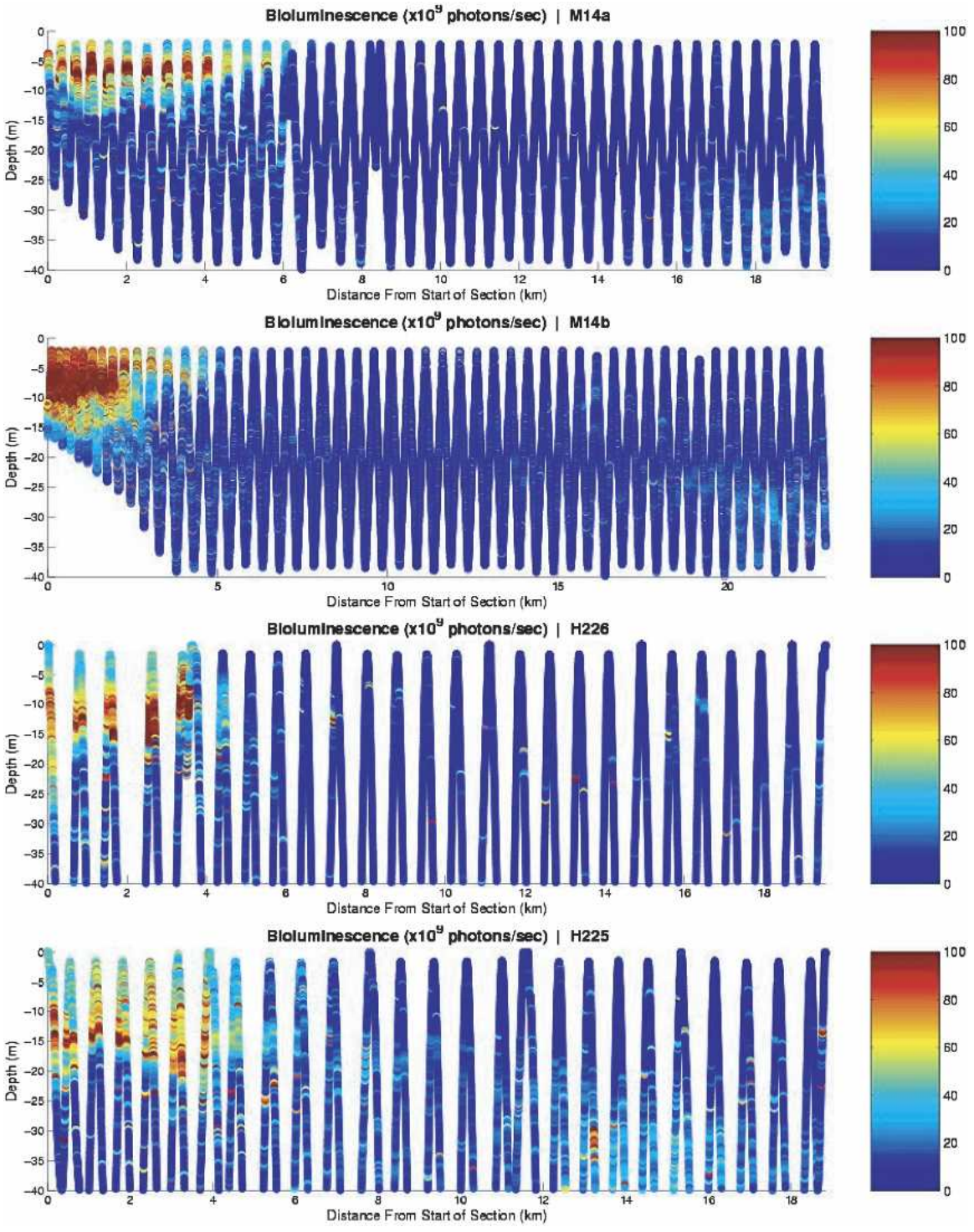

FIG. 4. Observed bioluminescence distributions along cross sections in Monterey Bay during Aug 2003. The distance scale starts from the onshore end of the sections.

present in the environment. This component is the bioluminescence that we are modeling.

Figure 4 shows observed BL distributions along four sections. Two of them are in the southern portion of the bay (see map on Fig. 1): the section labeled H225 was taken on 13 August, while H226 was taken on 14 August. The other two sections labeled M14a and M14b in the northern part of the bay were taken on 14 August.

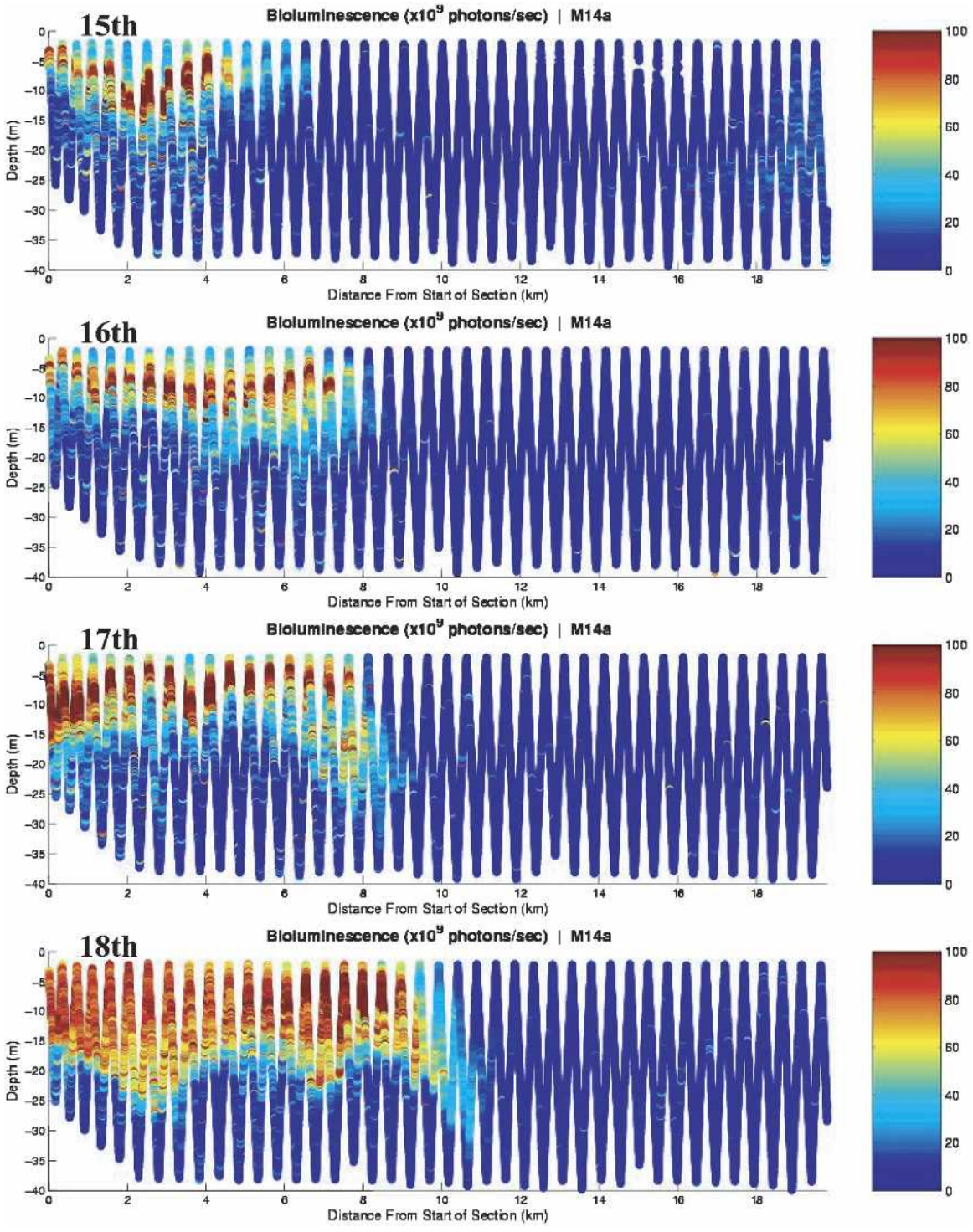

FIG. 5. Observed bioluminescence distributions along cross section M14a during 15–18 Aug 2003. The distance scale starts from the onshore end of the section.

The observed BL distributions (in 10^9 photons per second) are shown as a function of depth and distance offshore.

Another set of BL data used in this study is presented in Fig. 5. It shows the spatial and temporal change in the BL intensity over 4 days (15–18 August 2003) at section M14a (see Fig. 1). Figure 5 shows offshore spreading and intensification of observed BL intensity

over 3–4 days of upwelling-favorable conditions in the bay (see section 2 and Fig. 3).

4. Sensitivity studies and optimization of bioluminescence sampling

In Shulman et al. (2003), BL predictability experiments were conducted with the use of the advection–diffusion–reaction equation

$$\frac{\partial C}{\partial t} = -u\frac{\partial C}{\partial x} - v\frac{\partial C}{\partial y} - w\frac{\partial C}{\partial z} + \frac{\partial}{\partial x}\left(A\frac{\partial C}{\partial x}\right) + \frac{\partial}{\partial y}\left(A\frac{\partial C}{\partial y}\right) + \frac{\partial}{\partial z}\left(K\frac{\partial C}{\partial z}\right) + S(x, y, z, t), \tag{1}$$

where diffusivities (A and K) and velocities (u, v, w) are from the ICON and frsICON circulation models, and $S(x, y, z, t)$ is the source-minus-sink term for C. In this case BL is modeled as concentration C. For initialization, available BL observations are constantly assimilated into the model (1) by using the source term $S(x, y, z, t)$ in the following form (Shulman et al. 2003):

$$S(x, y, z, t) = \gamma(C - C^0)\delta(\tau - \tau^0), \tag{2}$$

where C^0 are BL observations, γ is the scalar nudging coefficient multiplying $(C - C^0)$, τ is the location in the model domain with coordinates (x, y, z), τ^0 is the location of the observed BL (C^0) with coordinates (x^0, y^0, z^0), and $\delta(\tau - \tau^0)$ is a Dirac function for which $\delta = 1$ when $\tau = \tau^0$ and $\delta = 0$ for all other cases.

Velocities and diffusivities in (1) are taken from the initialization day and kept unchanged during the initialization–assimilation procedure. In this case, the assimilated BL is spread throughout the model domain until the equilibrium is reached [when the value of dC/dt is zero in Eq. (1)]. This provides the initial BL distribution, which is dynamically balanced with the physical conditions at the time of the initialization.

According to (1), the following equilibrium relation is reached at the end of initialization:

$$-u_i\frac{\partial C_i}{\partial x} - v_i\frac{\partial C_i}{\partial y} - w_i\frac{\partial C_i}{\partial z} + \frac{\partial}{\partial x}\left(A_i\frac{\partial C_i}{\partial x}\right) + \frac{\partial}{\partial y}\left(A_i\frac{\partial C_i}{\partial y}\right) + \frac{\partial}{\partial z}\left(K_i\frac{\partial C_i}{\partial z}\right) + \gamma(C_i - C^0)\delta(\tau - \tau^0) = 0, \tag{3}$$

where C_i is equilibrium tracer distribution; subscript i means that variables are taken from the model predictions for the day of initialization. The equilibrium field C_i is used as the initial tracer distribution for the following 3 days' prognostic calculations with tracer Eq. (1) where the source-minus-sink term (S) is the last term on the left-hand side of Eq. (3) [note that the source-minus-sink term (S) is not equal to zero at the end of initialization procedure according to Eq. (3)].

During prognostic calculations, the hydrodynamic velocities and diffusivities change in accord with the hydrodynamic model.

On the open boundary of the model domain, the background BL values (minimum of observed BL) are advected into the model domain in the case of inflow, and the internal (one grid inside) BL values are advected to the open boundary in the case of outflow [see Shulman et al. (2003) for more details about initialization and prognostic simulations].

One of the well-known approaches for sensitivity studies and optimization of sampling strategies is based on the adjoint of the model (see, e.g., Baker and Daley 2000; Rabier et al. 1996; Errico 1997). Also, in McGillicuddy et al. (1998), the adjoint to the tracer model was used for estimation of the sources and sinks of the population dynamics. Here the adjoint code to the advection–diffusion–reaction model (1) was used to study the sensitivity of the modeled BL distributions to the sampling strategies of BL intensity.

The BL forecast measure should be defined for a quantification of the model forecast and for a sensitivity study. The forecast measure J can be any scalar function of initial conditions such that its gradient exists. It might be a function representing a weighted integration of C over a particular cross section. With the weight equaling 1, the forecast measure will be just the integral of the concentration. If the weight is velocity normal to the section, the forecast measure will be the flux of concentration through the section. "Intuitively," the flux of the concentration through the cross section better represents the influence of advective and diffusive processes on concentration distributions than just the integral of the concentration. The integrated flux of the concentration through a cross section in the bay was introduced as forecast measure J in our sensitivity studies,

$$J = \frac{\int_0^T \int_A Cu_n \, dA \, dt}{\int_0^T \int_A |u_n| \, dA \, dt}, \tag{4}$$

where A is cross section, u_n is velocity normal to the cross section A, and T is time length of the forecast (1–3 days). Note that J can be either positive or negative: although C is positive definite, the flux can be of either sign, depending on the orientation of the velocity

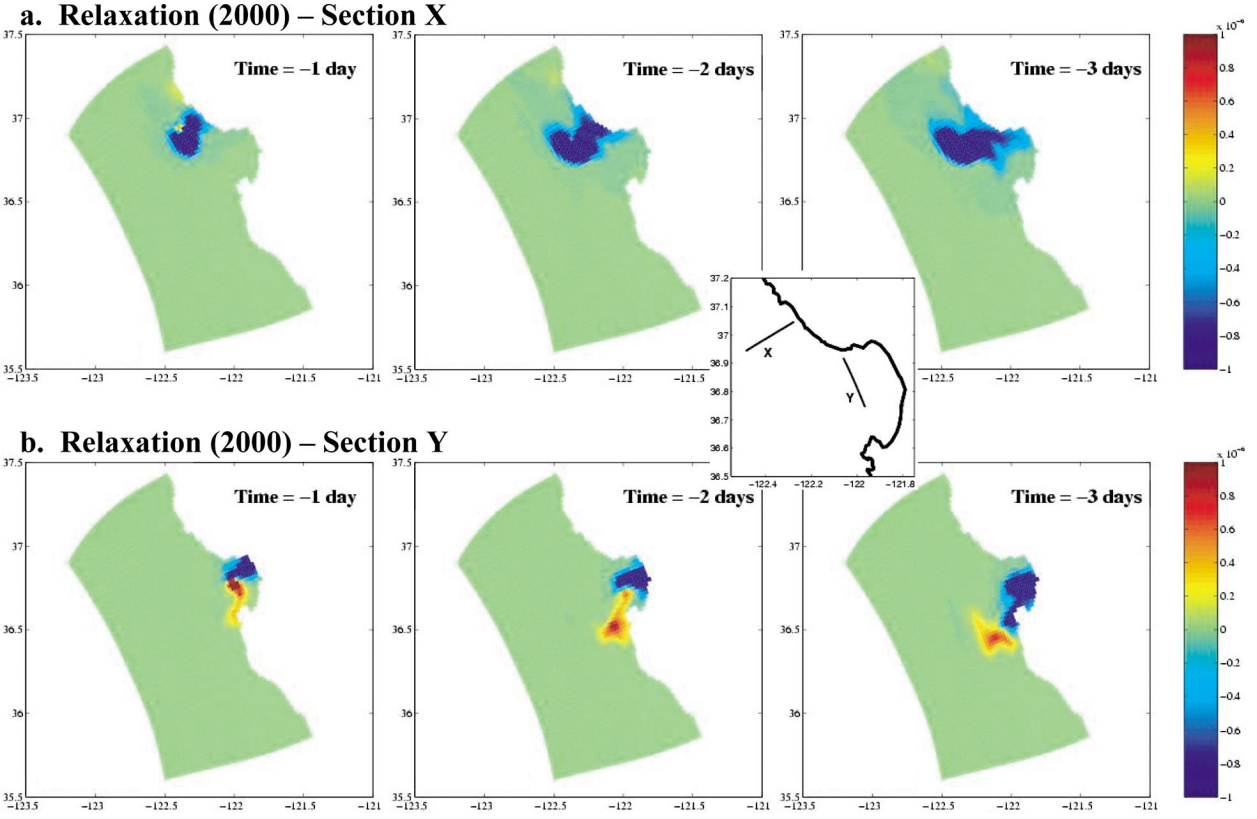

FIG. 6. Adjoint-based sensitivity maps for 1–3 days prior to the forecast during the relaxation event in Aug 2000 (a) at section X north of the bay; (b) at section Y in the northern part of the bay mouth.

through the section. By using the adjoint we estimate the gradient of the forecast measure J (4) with respect to the BL initial intensity at 12-h intervals prior to the forecast by

$$s = \frac{\partial J}{\partial C_0}, \tag{5}$$

where s is the sensitivity, C_0 is the initial three-dimensional distribution of BL, and $(\partial J/\partial C_0)$ is the gradient of J with respect to initial conditions C_0. In areas where the gradient of J has large positive or large negative values, a change in the BL intensity would have created a large impact on the forecast. Similarly, in areas where the gradient is small, such a change in the initial conditions would have very little effect on the subsequent forecast. Maps of the forecast measure gradients (5) show the sensitivity of the forecast to the BL distributions prior to the forecast. In other words, they show areas where initial conditions are most influential on the forecast and where sample BL intensity is most critical.

Derivation of adjoint-based sensitivity maps does not depend on the actual BL observations; therefore, optimal locations of BL sampling can be estimated prior to the actual measurements.

Here, we demonstrate sensitivity maps for the relaxation event during August 2000 and the upwelling event in August 2003. Maps of the sensitivity to the initial BL distributions for 1–3 days prior to the forecast during the relaxation event of 2000 are shown in Figs. 6a and 6b for two sections: the X section is outside of the bay, and the Y section is inside of the bay. Large positive values, in red, indicate a significant increase in the forecast measure J if BL intensity increases in this area, while large negative values, in blue, indicate a significant decrease in the forecast measure J if BL intensity increases in this area. As we have noted before, it is important to sample both areas where absolute value of the sensitivity metric is high.

Structure in the positive and negative regions of the sensitivity metric also contains useful information about the propagation of information within the system. Current structure during the relaxation event (Fig. 2) indicates a predominantly northward flow (at least down to 50 m) across section X (Fig. 6a). At the same time, the positive direction of velocity is defined as

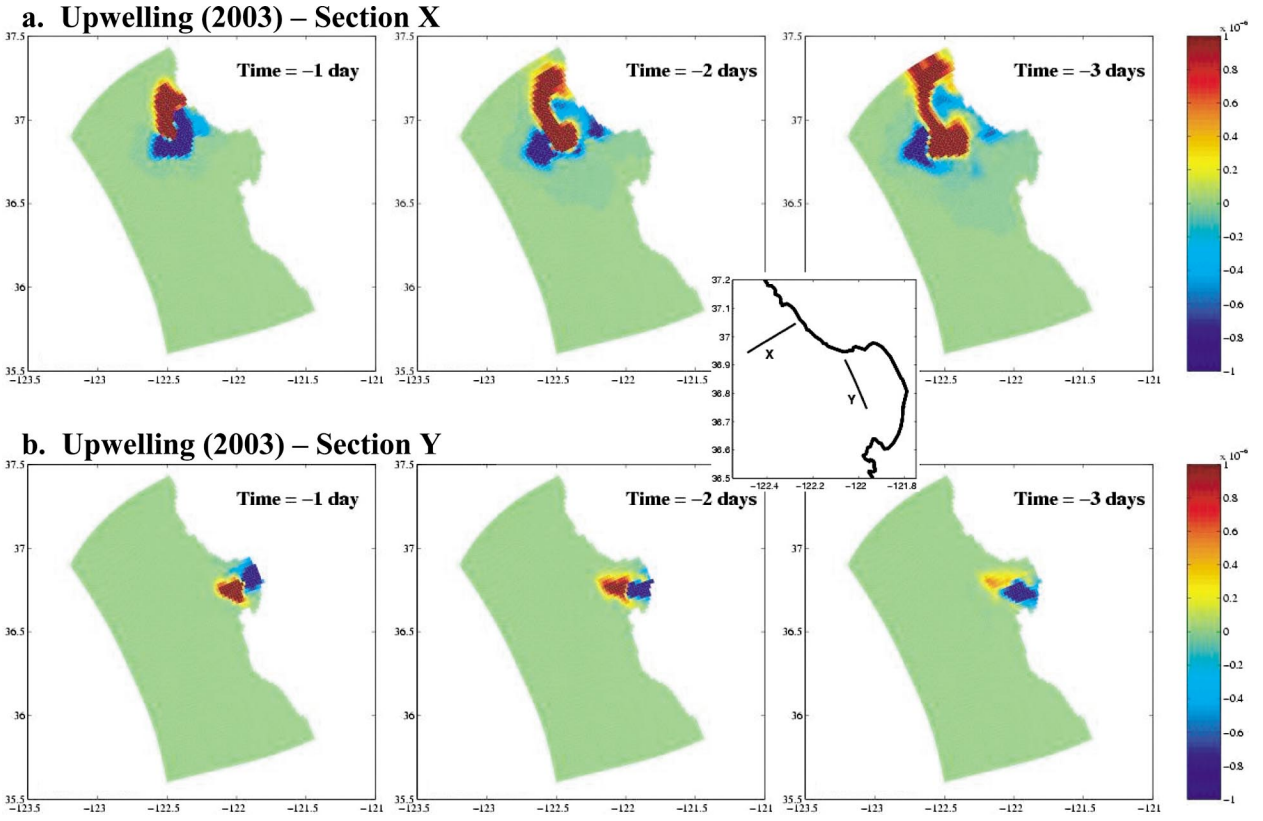

FIG. 7. Adjoint-based sensitivity maps for 1–3 days prior to the forecast during the upwelling event in Aug 2003 (a) at section X north of the bay; (b) at section Y in the northern part of the bay mouth.

southward in the model. Therefore, any increase in concentration C to the south of section X will contribute negative values of product Cu_n into the integrand of (4), and therefore decrease the value of J. This relationship is why the gradient [sensitivity metric (5)] has large negative values to the south of section X. Note that the sensitivity maps provide us with estimates as to the extent of the area to which BL sampling is needed 1, 2, or 3 days prior to the forecast. These regions for optimizing sampling cannot be deduced using only the current structure alone. For section Y (Fig. 6b), the direction of currents has more variability than at section X, and for this reason there are areas of negative and positive sensitivity. For section X, the maps (Fig. 6a) show high sensitivity to BL intensity in the northern part of the bay in the case of 2- and 3-day forecasts. This corresponds to the BL predictability results outlined in Shulman et al. (2003), when the assimilation of only the inside-the-bay survey data into the tracer model gave a good reconstruction of the observed location of the BL maximum for the outside-the-bay section. At the same time, for section Y, the critical areas for sampling are inside the bay and to the south of the bay. Sampling to the north and outside of the bay is not important for short-term BL predictions inside the bay. Again, this is in agreement with the results of short-term BL predictability experiments described in Shulman et al. (2003), in which it was demonstrated that assimilation of observations to the north of the bay has little or no effect on short-term predictions of BL features observed along the section inside the bay.

Sensitivity maps for the upwelling event of August 2003 are shown in Fig. 7. For a section inside the bay, it is critical to sample inside the bay and along the entrance to the bay. Sensitivity patterns rotate clockwise if we move from 1 day to 3 days prior to the forecast. This result indicates that sampling should be done inside the bay counterclockwise in time, which is supported by the presence of a strong cyclonic eddy inside the bay (Fig. 3).

5. Bioluminescence predictability experiments during the upwelling event of August 2003

To test the sampling strategy indicated by the sensitivity map in Fig. 7b, numerical experiments of the BL predictability were conducted for the period 14–17 August 2003. For the initialization of the advection–

diffusion–reaction model (1) on 14 August 2003, BL observations were assimilated into the model (1), while velocities and diffusivities from frsICON model predictions on 14 August were kept unchanged during the initialization procedure (see section 4). This procedure provides the initial BL distribution, which is dynamically balanced with the physical conditions on 14 August. Three numerical modeling experiments are presented here. Experiments differ in BL observations used for initialization of the model on 14 August. After initialization, for all experiments, 3 days of prognostic simulations [when physical fields in (1) change in accord with frsICON velocities and diffusivities] were conducted. Model predictions along section M14a during 15–17 August 2003 were compared to the corresponding BL observations (Fig. 5).

a. Experiment 1

Only BL observations from section M14a were assimilated for initialization of the model (Fig. 4, top). Therefore, BL intensity only from the section of interest in the model forecast over the next three days was used in the initialization. Information from the adjoint sensitivity map (Fig. 7b) was not used in this experiment. The experiment simulates the situation that assumes that BL variability is mostly determined by the intensity level of BL in the area where we are interested in forecasting.

b. Experiment 2

Bioluminescence observations from the three sections M14b, H225, and H226 were assimilated for initialization of the model. This experiment simulates the following situation: according to the sensitivity maps of Fig. 7b, BL sampling is conducted on 14 August along three sections, where the forecast sensitivity is high; however, we did not sample the area (section M14a) where we are interested in forecasting. In this case, we suppose that BL intensity is determined mostly by the advection–diffusion of the organisms from other areas in the modeling domain, and, therefore, BL intensity prior to the forecast sampled in the area of interest is not very important for 1–3-day forecasts.

c. Experiment 3

Bioluminescence observations from all four sections of Fig. 4 (M14a, M14b, H225, and H226) were assimilated for the initialization of the model. This experiment simulates the situation when BL sampling is conducted on 14 August along three sections, where the forecast sensitivity is high according to sensitivity maps (Fig. 7b), as well as along section M14a, where we are interested in predictions. In this experiment, we test the case when BL intensity sampling is conducted in the area of the forecast as well as in the most sensitive areas according to sensitivity maps of Fig. 7b.

Model-predicted BL intensity along section M14a is shown for all three experiments in Fig. 8, and surface-predicted model BL intensity is shown in Fig. 9. These distributions were compared to the observations of BL intensity along M14a shown in Fig. 5. In experiment 1, the predicted BL intensity remains very similar to the initial distribution on 14 August. With some changes in intensity, BL is concentrated in the area around 6 km offshore on all three days (Fig. 8). The model in experiment 1 did not predict observed offshore translation and intensification of BL intensity (Fig. 5).

In experiment 2 (Fig. 8), the model-predicted BL intensity indicates observed offshore spreading and intensification of BL intensity (Fig. 5) along section M14a. Though the level of model-predicted BL intensity is lower than the observed level, the results of experiment 2 support the sampling strategy derived from adjoint sensitivity maps of Fig. 7b. Finally, in experiment 3 (Fig. 8), the best agreement between model-predicted and observed BL intensity is achieved. This means that the BL sampling according to the adjoint sensitivity map, as well as in the area of interest (section M14a), provides BL predictions that agree with the observed in spatial and short-term temporal changes.

In experiment 3, Fig. 8 indicates the development of the secondary, offshore maximum during the third day of predictions. This secondary maximum is not present in the observations (Fig. 5). The second maximum represents the BL intensity advected from the north to the center of the bay (Fig. 9). The presence of this offshore maximum may be the result of slight deviation of the model-predicted southward jet from its true location. At the same time, in the case of longer-term predictions [O(7 days)], the lack of biological interactions influencing the BL distributions might well be a contributor to the development of this secondary maximum.

To quantify predictive skills in the experiments considered above, correlations between model-predicted and observed BL distributions at section M14a were calculated. Table 1 presents correlation coefficients between measurements taken during 14–17 August (Fig. 5) and model initial BL distributions (14 August, top row of Fig. 8), while Table 2 presents correlations between observed and model-predicted BL distributions during 14–17 August. Therefore, Tables 1 and 2 provide comparisons of persistence versus forecast for each of the predictive experiments described above. Overall for all experiments, the forecast has higher correlations

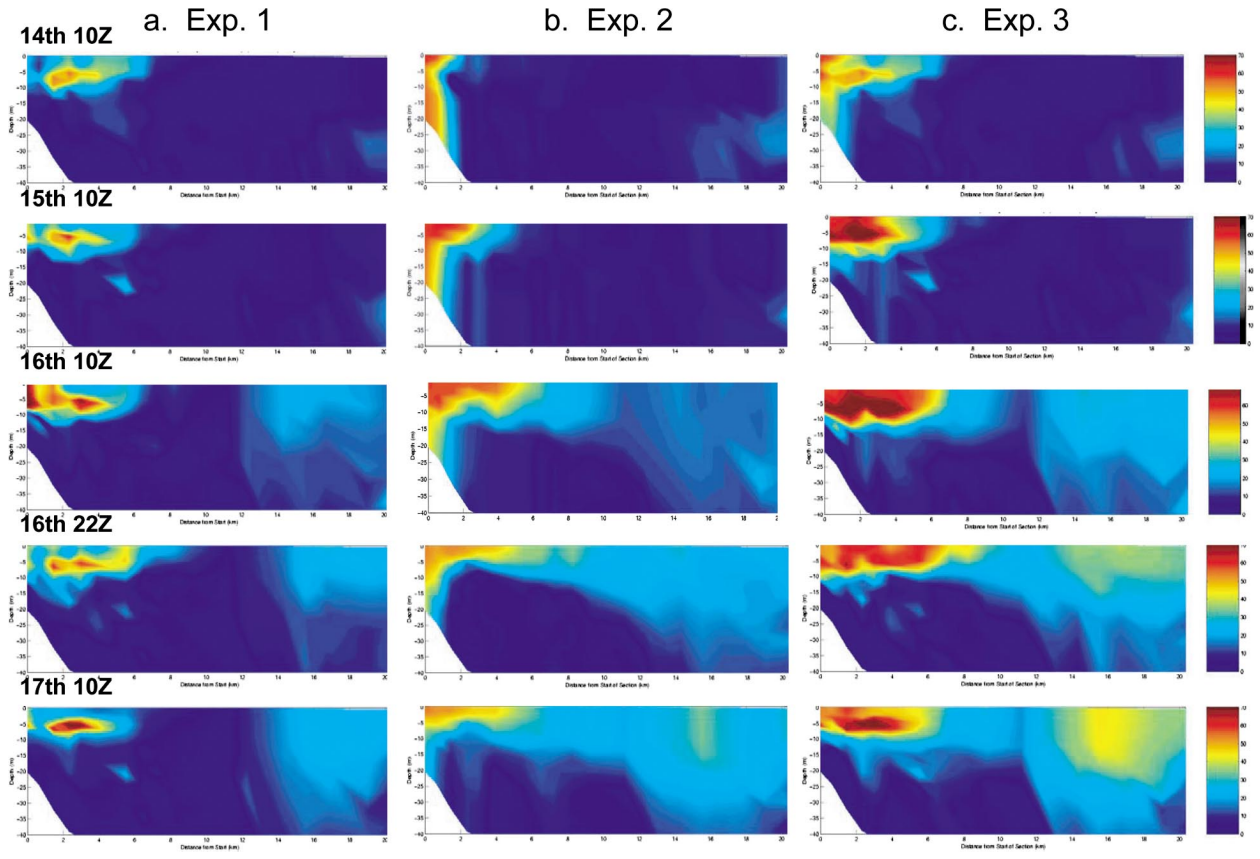

FIG. 8. Model-predicted bioluminescence distributions along section M14a. The distance scale starts from the onshore end of the section.

with observations than the persistence. For example, in experiment 2 (second row in Table 1), there are low correlations between the model initial and observed BL distributions during 14–17 August. This is due to the lack of assimilation of observed BL at section M14a on 14 August for the model initialization in experiment 2. However, the forecast in experiment 2 (Table 2) has much higher correlations with observations than the persistence (Table 1), especially for the first two days. Note that the presence of the secondary offshore BL maximum reduced the correlation between the model forecast and observed BL distribution for experiment 3 on 17 August.

6. Conclusions, discussion, and future plans

It has been demonstrated that the assimilation of BL observations into the advection–diffusion–reaction model provides a valuable methodology for the interpretation and short-term predictions of temporal and spatial changes in coastal bioluminescence. Short-term changes in observed BL intensity during wind relaxation (August 2000) and upwelling (August 2003) events were successfully predicted with the advection–diffusion–reaction model using velocities and diffusivities from the high-resolution circulation model of Monterey Bay. For successful short-term BL predictions, the optimization of locations and time of BL observations prior to the forecast is critical. Sensitivities of short-term BL forecasts to the sampling strategies were investigated by using the adjoint to the advection–diffusion–reaction model code. During the relaxation event, sensitivity maps of BL forecasts show that for short-term BL intensity predictions at the cross section inside of Monterey Bay, the area to the south of the bay (Fig. 6b) should have priority when sampling. During the upwelling event, sensitivity maps of BL forecasts suggest a counterclockwise strategy for sampling BL intensity inside the bay (Fig. 7b). Adjoint-based sensitivity maps provide a simple methodology for the optimization of BL sampling. Derivation of adjoint-based sensitivity maps does not depend on the actual BL observations; therefore, optimal locations of BL sampling

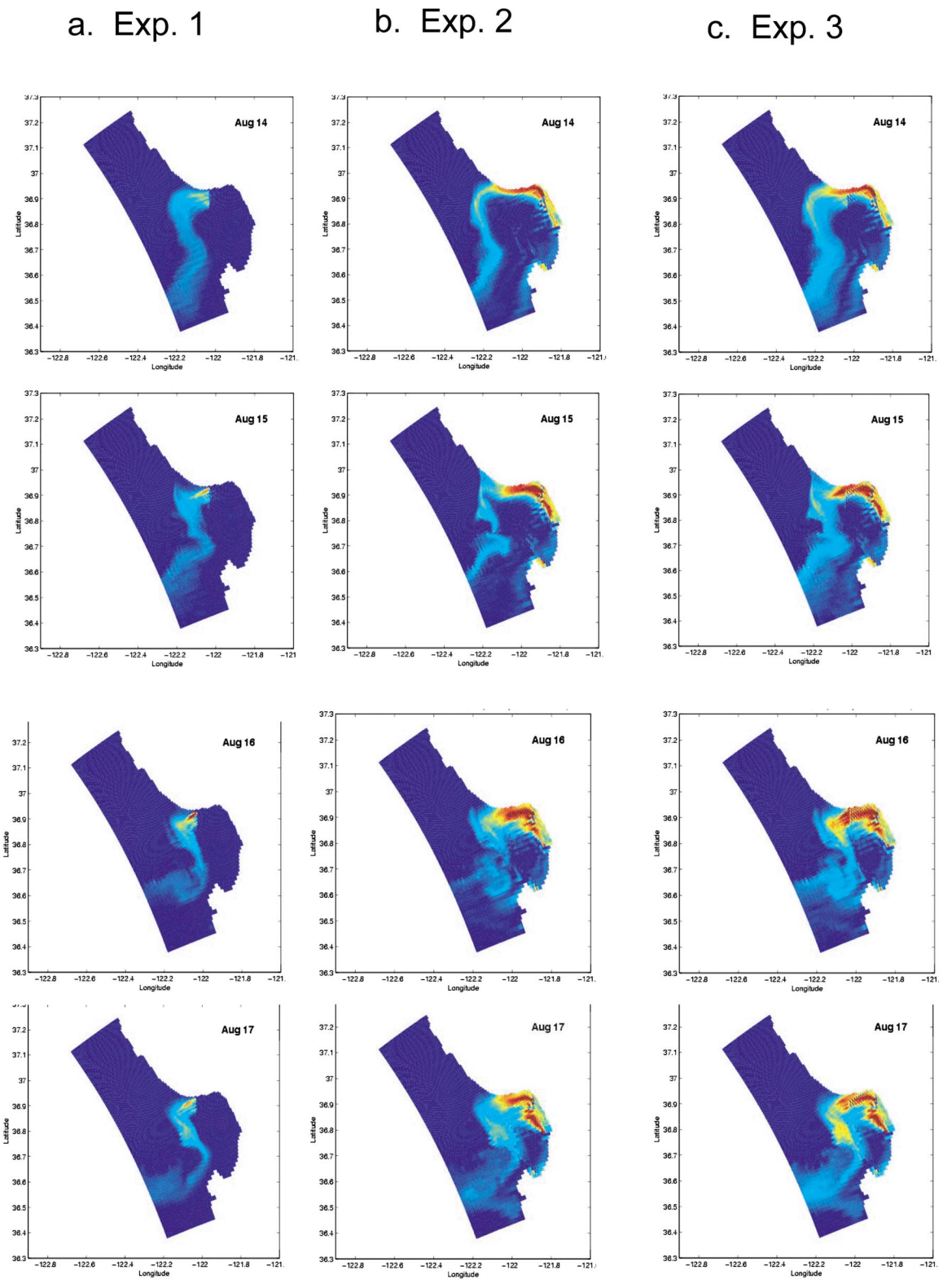

FIG. 9. Surface model-predicted bioluminescence distributions in three numerical experiments.

TABLE 1. Correlations between observed and model-predicted initial BL distributions.

	14 Aug	15 Aug	16 Aug	17 Aug
Experiment 1	0.79	0.48	0.57	0.54
Experiment 2	0.35	0.33	0.33	0.33
Experiment 3	0.79	0.63	0.64	0.62

can be estimated prior to the actual observations as long as the hydrodynamic field is known a priori.

Our results demonstrate a strong dependence of BL intensity distribution on flow conditions. During a relaxation event, patterns of cross-section velocities from the frsICON model indicated the development of a sharp frontal structure that moved onshore over 3 days. The observed BL intensity during these days also showed onshore translation, shallowing, and intensification of the BL (see Fig. 2 in Shulman et al. 2003). Bioluminescence observations during the upwelling of August 2003 (Figs. 4 and 5) indicate offshore translation and intensification of BL intensity along section M14a. Cross-section velocities from the frsICON model at section M14a show offshore translation of a strong frontal structure in the velocity field (Fig. 10). Therefore, during the relaxation event, the BL intensity maximum was moving onshore with the velocity front, while during the upwelling event the BL intensity maximum was moving offshore with the velocity front.

The proposed methodology for short-term BL predictions consists of the following:

1) setting up the circulation model for the area of interest and conducting 24–72-h forecasts of physical conditions;
2) sampling of BL intensity according to adjoint-based BL sensitivity maps;
3) dynamical initialization (section 4; Shulman et al. 2003) of the tracer model when BL observations are assimilated into the tracer model while velocities and diffusivities are kept unchanged during the initialization process (this dynamic initialization procedure provides an equilibrium tracer distribution that is balanced with the velocity and diffusivity fields from the circulation model);
4) using the equilibrium BL distribution as the initial BL field for 3 days of prognostic calculations when velocities and diffusivities evolve in accord with the circulation model dynamics.

TABLE 2. Correlations between observed and model-predicted BL distributions.

	14 Aug	15 Aug	16 Aug	17 Aug
Experiment 1	0.79	0.63	0.54	0.60
Experiment 2	0.35	0.54	0.63	0.45
Experiment 3	0.79	0.67	0.7	0.6

The numerical bioluminescence predictability experiments demonstrated a close agreement between observed and model-predicted short-term spatial and temporal changes of the coastal bioluminescence. Our results also indicate that advective–diffusive processes largely explain the short-term evolution of BL intensity. At the same time, it is clear that advective–diffusive processes cannot explain the full spatial and temporal variability of BL intensity. Source and sink terms representing ecological interactions, especially for relatively long-term predictions [O(7 days)], should be included. In experiment 3, the secondary, offshore, unobserved maximum developed during the third day of predictions. The lack of biological interactions influencing the BL distributions might be at least a partial contributor to the development of this secondary maximum.

Derivation and parameterization of bioluminescence sources and sinks represent a very challenging problem: the complex interactions characterizing life cycles of autotrophs, grazers, and predators producing BL, and, especially, the mathematical parameterizations and formulations of the biological processes governing BL variability in complex ecosystems are fundamental research issues. In McGillicuddy et al. (1998) the sources and sinks of the population dynamics (right-hand term in the advection–diffusion–reaction tracer equation) were determined by inversion of the advection–diffusion–reaction tracer equation. Observations from 11 yr of sampling were used for inversion, verification, and interpretation of population dynamics maps derived from the inversion. Our future research will include the design and execution of similar inversion experiments to determine sources and sinks of BL intensity in Monterey Bay. The adjoint model developed for the ICON model tracer routine will be the basis for these inversion experiments. The results of these inversion experiments, together with research presented here, will provide an understanding of the relative contributions of advective–diffusive versus biological processes to short-term and relatively long-term [O(7 days)] variability of BL intensity in the bay. An important tool for achieving this level of understanding will be the Coupled Physical BioOptical Model (http://www7320.nrlssc.navy.mil/cobiopp/), as used for the interpretation of bioluminescence inversion experiments and for the development of numerical parameterizations of bioluminescence sources and sinks.

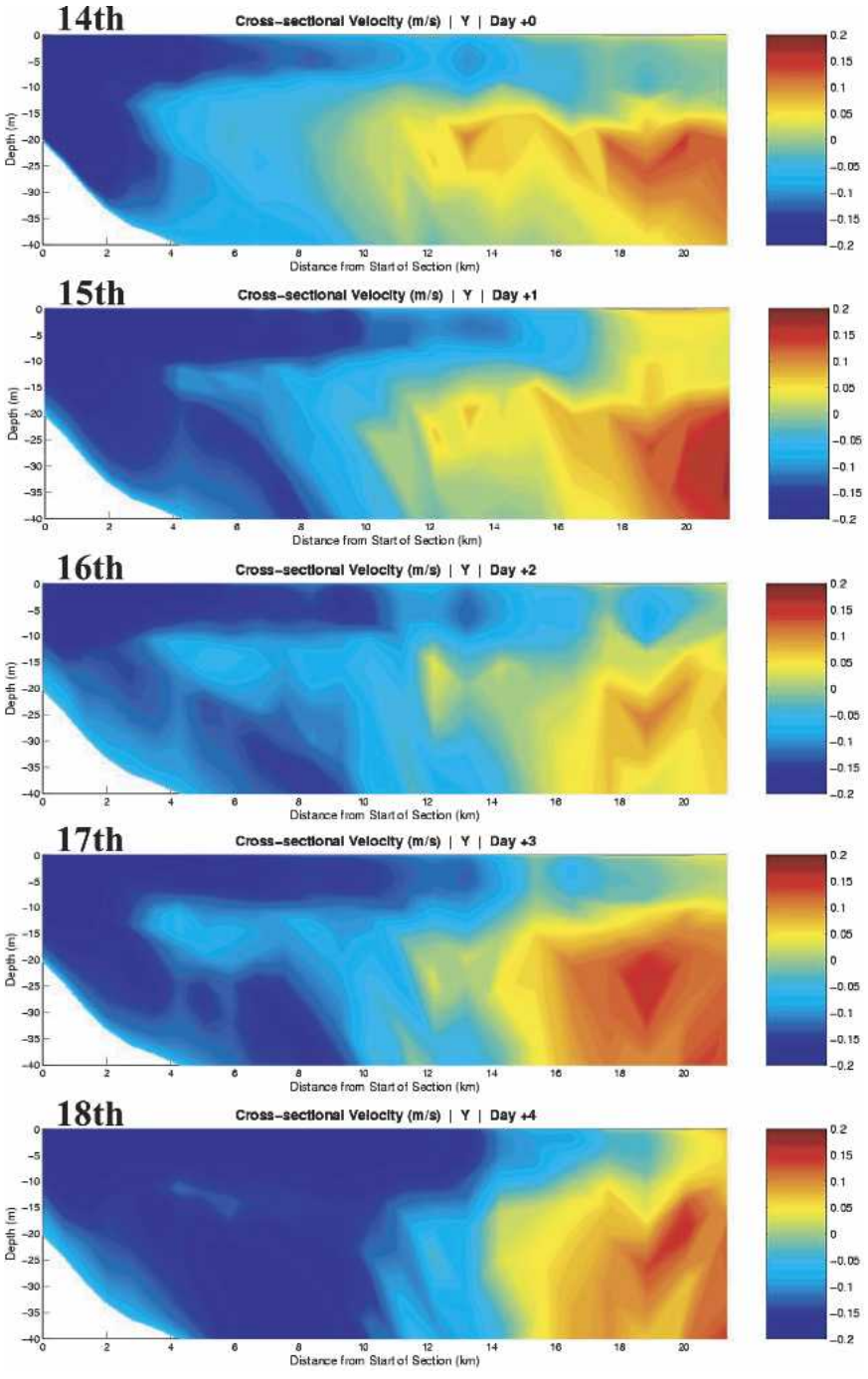

FIG. 10. ICON-model-predicted cross-section velocities along section Y. Positive cross-sectional velocity is from southwest to northeast across section Y. The distance scale starts from the onshore end of the section.

Acknowledgments. This work has been supported by the Ocean Optics and Biology and Physical Oceanography Programs of the Office of Naval Research. Shulman's support is through the NRL "Use of a Circulation Model to Enhance Predictability of Bioluminescence in the Coastal Ocean" project sponsored by the Office of Naval Research. We are grateful to MBARI's AUV team and the crews of the R/V *Zephyr* and R/V *Paragon* for their efforts during operations at sea. We thank Alan Weidemann and Bob Arnone for helpful

discussions and support. The authors thank Shelley Blackwell, Jodi Brewster, Cristina Orrico, and Christy Herren for help with bioluminescence data. We thank Sergio deRada and Stephanie Anderson for processing atmospheric forcing and open boundary conditions for the ICON and PWC models. Our thanks go to the AOSN II interdisciplinary group for many helpful discussions. Computer time for the numerical simulations was provided through a grant from the U.S. Department of Defense High Performance Computing Initiative.

REFERENCES

Baker, N. L., and R. Daley, 2000: Observation and background adjoint sensitivity in the adaptive observation-targeting problem. *Quart. J. Roy. Meteor. Soc.,* **126,** 1431–1454.

Blumberg, A., and G. L. Mellor, 1987: A description of a three-dimensional coastal ocean circulation model. *Three Dimensional Coastal Models*, N. S. Heaps, Ed., Coastal and Estuarine Sciences, Vol. 4, Amer. Geophys. Union, 1–16.

Errico, R. M., 1997: What is an adjoint model? *Bull. Amer. Meteor. Soc.,* **78,** 2577–2591.

Herren, C. M., A. L. Alldredge, and J. F. Case, 2004: Coastal bioluminescent marine snow: Fine structure of bioluminescence distribution. *Cont. Shelf Res.,* **24,** 413–442.

Hodur, R. M., 1997: The Naval Research Laboratory's Coupled Ocean/Atmosphere Mesoscale Prediction System (COAMPS). *Mon. Wea. Rev.,* **125,** 1414–1430.

Kindle, J. C., R. M. Hodur, S. deRada, J. D. Paduan, L. K. Rosenfeld, and F. Q. Chavez, 2002: A COAMPS reanalysis for the eastern Pacific: Properties of the diurnal sea breeze along the central California coast. *Geophys. Res. Lett.,* **29,** 2203, doi:10.1029/2002GL015566.

McGillicuddy, D. J., Jr., D. R. Lynch, A. M. More, W. C. Gentleman, C. S. Davis, and C. J. Meise, 1998: An adjoint data assimilation approach to diagnosis of physical and biological controls on Pseudocalanus spp. in the Gulf of Maine–George Bank region. *Fish. Oceanogr.,* **7** (3/4), 205–218.

Moline, M. A., and Coauthors, 2005: Remote environmental monitoring unit (REMUS): An autonomous vehicle for characterizing coastal environments. *J. Atmos. Oceanic Technol.,* **22,** in press.

Paduan, J. D., and I. Shulman, 2004: HF radar data assimilation in the Monterey Bay area. *J. Geophys. Res.,* **109,** C07S09, doi:10.1029/2003JC001949.

Rabier, F., E. Klinker, P. Courtier, and A. Hollingsworth, 1996: Sensitivity of forecast errors to initial conditions. *Quart. J. Roy. Meteor. Soc.,* **122,** 121–150.

Rosenfeld, L. K., F. B. Schwing, N. Garfield, and D. E. Tracy, 1994: Bifurcated flow from an upwelling center: A cold water source for Monterey Bay. *Cont. Shelf Res.,* **14,** 931–964.

Shulman, I., C.-R. Wu, J. K. Lewis, J. D. Paduan, L. K. Rosenfeld, J. C. Kindle, S. R. Ramp, and C. A. Collins, 2002: High resolution modeling and data assimilation in the Monterey Bay area. *Cont. Shelf Res.,* **22,** 1129–1151.

——, S. H. D. Haddock, D. J. McGillicuddy Jr., J. D. Paduan, and W. P. Bissett, 2003: Numerical modeling of bioluminescence distributions in the coastal ocean. *J. Atmos. Oceanic Technol.,* **20,** 1060–1068.

Wilcox, J. S., J. G. Bellingham, Y. Zhang, and A. B. Baggeroer, 2001: Oceanographic surveys with autonomous underwater vehicles: Performance metrics and survey design. *J. Oceanic Eng.,* **26,** 711–725.